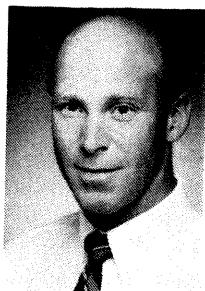


Flight Measurements of Blade-Vortex Interaction Noise Including Comparisons With Full-Scale Wind Tunnel Data



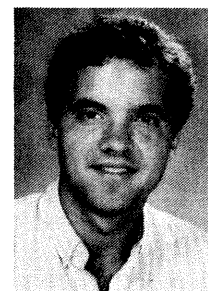
Gloria K. Yamauchi



David B. Signor

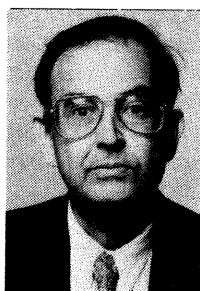


Michael E. Watts



Francisco J. Hernandez

*Aerospace Engineers
NASA Ames Research Center
Moffett Field, California*



Philip LeMasurier
*Senior Technical Engineer
Sikorsky Aircraft, Subsidiary of UTC
Trumbull, Connecticut*

Acoustic measurements of a Sikorsky S-76C helicopter in flight were compared with acoustic measurements of a full-scale S-76 rotor tested in the 80- by 120-Foot Wind Tunnel at NASA Ames Research Center. The flight measurements were acquired using the NASA Ames YO-3A research aircraft fitted with acoustic instrumentation. Flight and wind tunnel data were compared for three conditions. For the low and moderate advance ratio conditions, the BVI pulse widths of the flight and wind tunnel data were very similar, indicating the conditions were well-matched. Comparisons between the flight and wind tunnel data waveforms for the high advance ratio case ($\mu \approx 0.25$) were poor. For this condition, the wind tunnel data showed greater blade-to-blade and revolution-to-revolution variability than the flight data. Effects of tip-path-plane angle and advance ratio on the BVI flight data were also analyzed. The flight data showed the BVI peaks increased with increasing tip-path-plane angle until reaching a maximum at an angle which varied with flight condition. Further increases in the tip-path plane angle resulted in BVI peak reduction. Increasing advance ratio increased the magnitude of the BVI noise for the flight conditions tested.

Notation

C_T rotor thrust coefficient, $\text{thrust}/\pi R^2 \rho (\Omega R)^2$
 SPL Sound Pressure Level using corrected pressure referenced to 20 μPa , dB
 SPL_{sl} Sound Pressure Level representing sum of energy in 1/3-octave bands with center frequencies from 100 Hz to 1000 Hz (using corrected pressure referenced to 20 μPa), dB
 f helicopter equivalent flat plate area, ft^2
 I_s helicopter shaft tilt offset (positive, shaft tilt rearward)
 M_{tip} hover tip Mach number, $\Omega R/(\text{sound speed})$
 p uncorrected pressure, Pa
 p_o static pressure of test condition, Pa
 p_{sl} corrected pressure referenced to standard atmosphere sea level

(sl) pressure, Pa
 $p_{\text{sl}o}$ standard atmosphere sea level (sl) pressure, Pa
 R rotor radius, ft
 V_D descent rate, ft/min (positive, descending)
 V_{true} true airspeed, kts
 α_{tip} rotor tip-path-plane angle, deg (positive, rotor plane tilt rearward)
 γ glide slope angle, $\sin^{-1}(V_D/V_{\text{true}})$, deg (positive, descending)
 μ advance ratio, $V_{\text{true}}/\Omega R$
 Ω rotor rotational speed, rad/s
 ρ density, slug/ ft^3
 ψ rotor azimuth angle, deg
 θ_f helicopter attitude measured by gyroscope, deg (positive, nose up)

Introduction

Blade vortex interaction (BVI) noise has been extensively studied over the years because of the particularly annoying and detectable nature

of the noise. The in-flight acoustic measurement method has played a key role in BVI research by providing data against which small-scale wind tunnel data and theoretical predictions have been compared.

The technique of acquiring acoustic measurements of helicopters in forward flight was developed over 15 years ago by Schmitz and Boxwell (Ref. 1), when noise measurements of a UH-1H were made using the OV-1C fixed wing aircraft as the "flying" acoustic platform. Vause et al. (Ref. 2) compared these measurements with 1/7-scale rotor data taken in the NASA Ames 7- by 10-Foot Wind Tunnel to investigate the scalability of high-speed impulsive noise. The acoustic waveforms were found to scale fairly well, establishing the validity of using small-scale data for the study of rotor high-speed impulsive noise, at least qualitatively. By 1980, the NASA Ames YO-3A research aircraft had been outfitted with acoustic instrumentation and subsequent in-flight measurements were made with this quiet aircraft. Boxwell and Schmitz (Ref. 3) conducted a flight test with the YO-3A and the two-bladed UH-1H and AH-1S helicopters. The investigation studied the differences in BVI noise of different main rotor blade sets. Schmitz et al. (Ref. 4) next compared the flight measurements of the AH-1S with 1/7-scale AH-1G/Operational Loads Survey rotor data acquired in the CEPRA-19 anechoic wind tunnel. The study showed that BVI was a scalable phenomenon for a two-bladed rotor provided the nondimensional parameters of thrust coefficient (C_T), advance ratio (μ), hover tip Mach number (M_{tip}) and rotor tip-path-plane angle (α_{tpp}) were matched between flight and wind tunnel tests. The same rotor was later tested in the aerodynamically cleaner and quieter Deutsch-Niederlaendischer Windkanal (DNW) open test section over a higher speed range. Spletstoesser et al. (Ref. 5) compared the high-speed impulsive noise from this small-scale test with the full-scale data of Ref. 3. A more in-depth study of BVI scalability using the same two data sets was next performed by Spletstoesser et al. (Ref. 6). BVI directivity and sensitivity to C_T , μ , M_{tip} , and α_{tpp} were investigated. The study showed that the BVI noise did not scale well at moderate to high advance ratios ($\mu > 0.22$).

BVI noise source location on the rotor disk and BVI noise directivity were studied in detail by Spletstoesser et al. (Ref. 7) and Martin et al. (Ref. 8), respectively. The subject rotor, a 40% dynamically scaled model of the BO-105 main rotor, was tested in the DNW. Traversing an array of microphones beneath the rotor plane generated a detailed directivity mapping. Blade-wake interactions and radiation patterns for a range of tip-path-plane angles and advance ratios were identified. As a result, Burley and Martin (Ref. 9) reported in detail the effects of tip-path-plane angle on BVI noise. Parametric (α_{tpp} and μ) effects on the movement of the strongest BVI noise radiation direction were determined by Martin et al. (Ref. 10) in a subsequent test in the DNW with the same rotor system. Other studies, for example, Marcolini et al. (Ref. 11), have been conducted using blade airloads data as input to analyses which

then predict BVI noise.

A review of the literature reveals a deficiency in full-scale flight measurements of BVI noise. Measurements exist for two-bladed rotors only. In addition to the UH-1H and AH-1S flight tests discussed earlier, Cross and Watts (Ref. 12) acquired BVI noise measurements of the two-bladed AH-1G as part of the Tip Aerodynamics and Acoustic Test.

The objective of NASA's In-Flight Rotorcraft Acoustics Program is to explain the similarities and differences between BVI noise measurements in flight and in the wind tunnel. The program should help establish the validity of using the 40- by 80-Foot and 80- by 120-Foot wind tunnels as acoustic testing facilities for full-scale rotor research. The attractive feature of this program is that no scaling of aerodynamic or acoustic phenomena is necessary since identical (geometric and dynamic) rotor systems can be tested in flight and in the wind tunnels.

This paper presents the results from an S-76 flight test, which is the first of a planned series of flight tests with four-bladed rotors. This test was conducted jointly with the Sikorsky Aircraft, Subsidiary of United Technologies Corporation. Effects of tip-path-plane angle and advance ratio on BVI noise are presented and compared with trends observed in previous small-scale wind tunnel and two-bladed rotor flight tests. Limited comparisons are made with acoustic measurements acquired in the 80- by 120-Foot Wind Tunnel.

Description of Test

S-76C Aircraft

The test aircraft was a Sikorsky S-76C helicopter. Features of the helicopter are provided in Table 1. The S-76 rotor system is composed of four blades with coincident flap and lag articulation provided at the blade root by elastomeric bearings. Blade pitch motion is permitted by the same bearings. Fig. 1 presents details of the rotor blade, which has a 22-ft radius with a 15.5-in nominal chord. Table 2 provides additional characteristics of the rotor system.

YO-3A Aircraft

The flight measurements were acquired using the NASA Ames YO-3A research aircraft fitted with acoustic instrumentation. The low tip speed of the nose-mounted propeller, a quiet belt-drive system, and a large muffler make the YO-3A a low-noise aircraft well suited for measuring in-flight helicopter noise. The YO-3A carries a pilot and flight engineer and is equipped with instrumentation for acoustic and flight condition data acquisition. Characteristics of the YO-3A are shown in Table 3. Further details about the YO-3A can be found in Cross (Ref. 13) and Cross and Watts (Ref. 14).

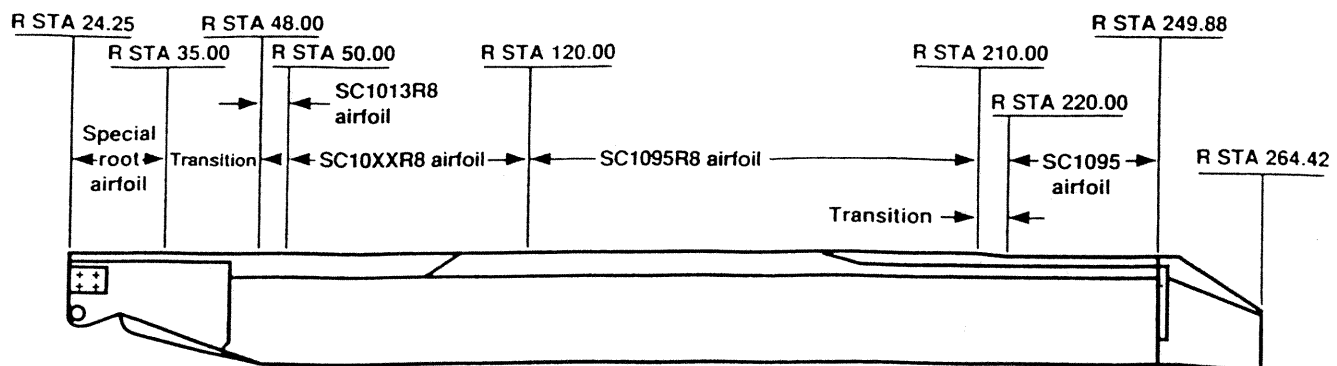


Fig. 1. S76C rotor blade features.

Table 1. S-76C Aircraft Characteristics

Aircraft Tail No.	N3123U
Empty weight with fuel	9797 lb
Fuel capacity	1850 lb
Max. cruise speed @ sea level	approximately 150 kts
Equivalent flat plate area	12.6 ft ²
Longitudinal c.g.	station 210 inches
Lateral c.g.	station 0.0 inches

Table 2. S-76C Rotor Characteristics

Main rotor	
Number of blades	4
Rotor radius	22 ft
Nominal chord	15.5 in
Solidity ratio	0.0748
Flapping hinge offset	3.79% radius
Lock number	11.6
Airfoils	SC1013-R8, SC1095-R8, SC1095
Normal operating rpm	313 (100% = 293 rpm)
Tail rotor	
Number of blades	4
Normal operating rpm	1723 (@ 313 main rotor rpm)

Table 3. YO-3A Aircraft Characteristics

Wingspan	57 ft
Length	29.3 ft
Height	9.1 ft
Maximum gross takeoff weight	3800 lb
Propeller diameter	100 in
Stall speed	60 kts (approx. IAS)
Maximum speed	110 kts (approx. IAS)
Power plant	210 hp (Continental)
Aircraft type	single engine, tail dragger
Number of propeller blades	3
Propeller tip speed	360 ft/s

Flight Measurements

YO-3A Data Acquisition System. The YO-3A has one-half inch condenser, free-field microphones mounted at each wingtip and at the top of the vertical tail. The microphones have diameters of 0.5 in and are fitted with bullet nose cones. A wing-mounted instrumentation boom provides indicated airspeed, altitude, outside air temperature, and angles of attack and sideslip. An analog tape recorder on board the YO-3A records the signals from the three microphones and the instrumentation boom. In addition, a time code and a once-per-revolution (1/rev) signal transmitted from the subject helicopter are recorded. The tape recorder voice channel is used to record flight condition parameters and pilots' comments for each flight test point. Once specified flight conditions are established, microphone gains are adjusted to insure maximum allowable signal response (2 V peak-to-peak); the gains are then hand-recorded. Signals are recorded continuously for 30 s at a tape speed of 30 in/s yielding a frequency range of DC to 20 kHz.

S-76C Data Acquisition System. A portable, eye-safe laser rangefinder was used from the passenger compartment of the S-76C to establish and maintain the desired separation distance from the YO-3A. A small section of the YO-3A starboard wing was used as a target for the laser. The distances were viewed using the heads-up display on the laser rangefinder and downloaded to a lap-top computer at a rate of 2

samples/s. The downloaded distance values were synchronized through the time code with the acoustic data recorded by the YO-3A data system. The capability of recording a time-accurate separation distance is a much-desired refinement to the previously used distance measuring technique. The helicopter attitude was measured by a gyro mounted on the floor of the S-76C and hand-recorded once during the 30 s of acoustic data recording.

Wind Tunnel Measurements

Acoustic measurements of a full-scale S-76 rotor were made in the 80- by 120-Foot Wind Tunnel at NASA Ames Research Center. Both the flight test and wind tunnel rotor blade systems were production S-76 systems, except for the one instrumented blade used in the wind tunnel. The rotor was mounted on the Rotor Test Apparatus (RTA). Fig. 2 shows the S-76 rotor and RTA installed in the wind tunnel. The RTA includes a rotor balance which measures rotor lift, drag, and side-force. Measurements from the rotor balance were sent through a 100 Hz low-pass filter and acquired over a 30 s period, along with the tunnel conditions, at a rate of approximately 148 samples/s. The microphone selected for flight comparison was located two rotor diameters upstream of the rotor hub, nominally 25 deg down from the rotor plane at an azimuth of 150 deg. The microphone was the same type used on the YO-3A and was mounted on an acoustically-treated and faired stand hard-mounted to the wind tunnel floor (see Fig. 2). Once test conditions were established, the microphone signal and rotor 1/rev signal were recorded continuously for a minimum of 30 s at a tape speed of 30 in/s yielding a frequency range of DC to 20 kHz.

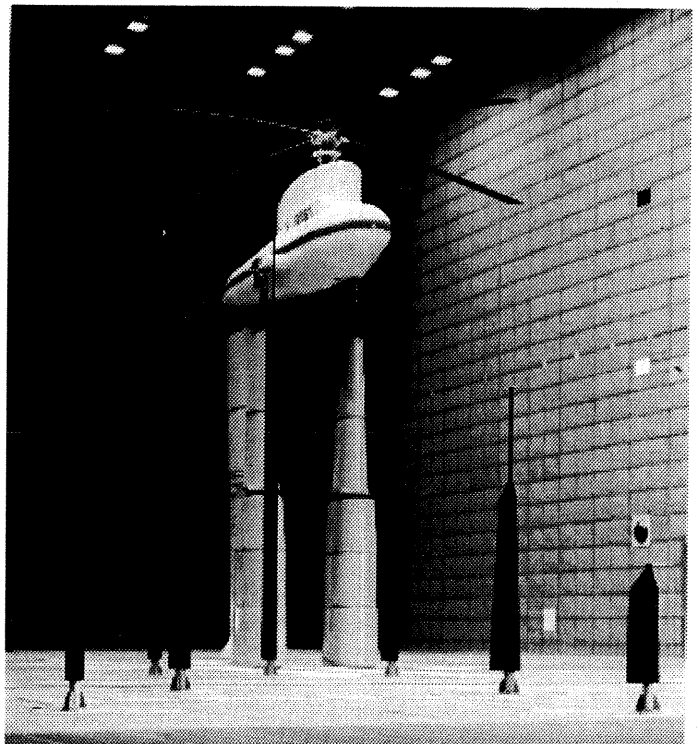


Fig. 2. S-76 rotor installation in the 80- by 120-Foot Wind Tunnel.

Flight Formation

The YO-3A tail-mounted microphone was selected as the primary microphone for wind tunnel comparison after considering limited S-76C

pilot visibility. Once the YO-3A pilot established the specified flight conditions, the S-76C was positioned such that the tail microphone was located in the desired position (two diameters upstream, nominally 25 deg down from the rotor plane, 150 deg rotor azimuth) relative to the hub. Figs. 3(a) and 3(b) present a plan and side view of the formation, respectively. The angular alignment of the two aircraft was established visually by the S-76C pilot who aligned the top of the YO-3A tail with a target on the right wing of the YO-3A. The desired aircraft separation distance was established using the laser rangefinder. Fig. 4 shows the "on condition" view from the passenger compartment of the S-76C. Fig. 5 is a photograph of the formation viewed from the side.

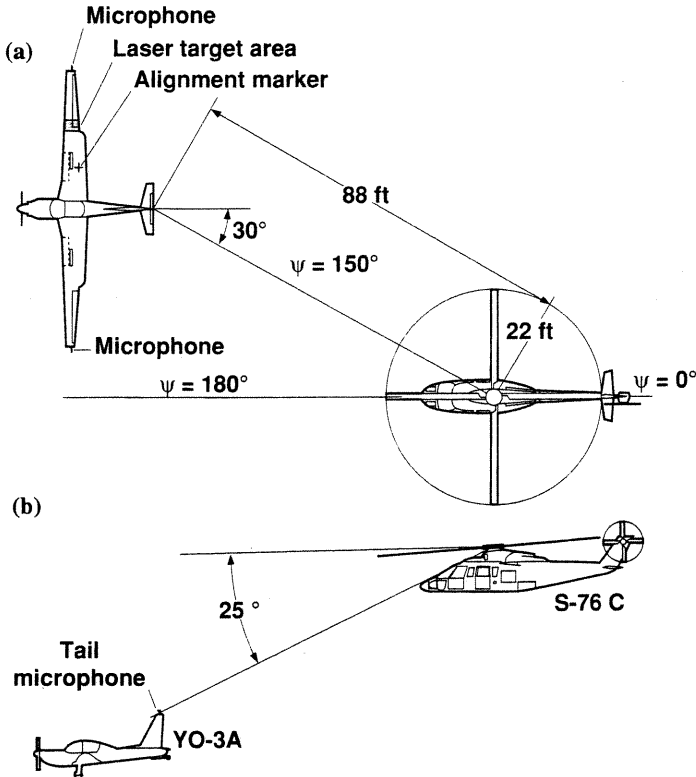


Fig. 3. Flight formation. (a) plan view (b) side view.

Data Reduction Procedure

Acoustic Data

The Acoustic Laboratory Data Acquisition System (ALDAS), a Macintosh-based software package developed at NASA Ames, was used to reduce the majority of the data. Capabilities and features of ALDAS are described by Watts (Ref. 15). The acoustic signals were passed through an analog 2500 Hz low-pass filter and then digitized for 10 s or approximately 50 rotor revolutions. The mean value of the rotor rpm, determined from the recorded 1/rev signal, was used to calculate a digitization rate insuring nominally 2048 samples/rev (approximately 10000 samples/s). A calibration signal generated by a pistonphone and recorded before every flight was used to convert the digitized acoustic signal to pressure units. Next, a time history of one rotor revolution representing an average of 32 revolutions was constructed.

Averaging was performed in the time domain. A marker or feature existing in each revolution of data is needed to perform the averaging. The usual choice for the marker is the 1/rev spike recorded every revolution. Unfortunately, the rotor rpm during flight varies with gusts and slight adjustments to the helicopter controls. In addition, small changes



Fig. 4. Formation view from helicopter passenger compartment.

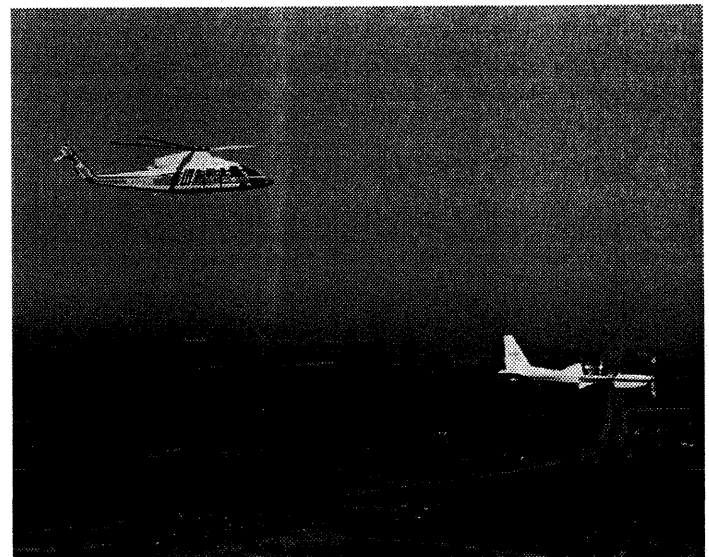


Fig. 5. Formation side view.

in the separation distance between the S-76C and YO-3A causes time shifts in the recorded noise measurements. Therefore, using the 1/rev spike as an averaging marker will introduce smearing of the signal during averaging. A typical time history from the YO-3A tail mounted microphone includes four multi-peak events, representing the four blades, per rotor revolution. Each event consists of two to four spikes, where each spike is caused by a single BVI. These BVIs occur along the span of the blade at nearly the same time and so are referred to collectively as a single "event." In order to present an averaged signal while retaining the salient features of the four events, a feature evident in each of the four events and repeated throughout a minimum of 32 revolutions was chosen as the marker for averaging. For example, the marker could be a

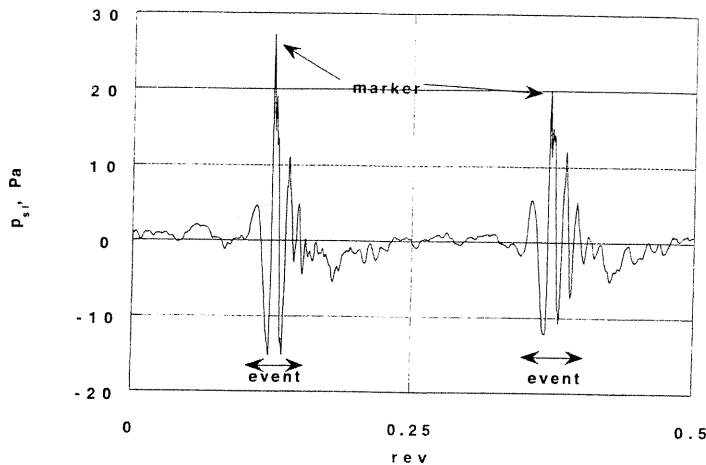


Fig. 6. Typical BVI time history features.

particular positive pressure peak. This marker may be different for different flight conditions. Fig. 6 presents two events for one-half of a rotor revolution. For this example, the large positive peak is chosen as the marker. This procedure is not unlike the method used in Ref. 5 in averaging high-speed impulsive noise time histories. Because the time between events was also not constant, each of the four impulsive events was averaged separately over 32 revolutions. A composite time history of one rotor revolution was then constructed by piecing together the four averaged events. Because of the averaging technique used, zero time is not equivalent to zero degrees rotor azimuth.

Following the method of Ref. 5, the acoustic pressures were corrected to standard atmosphere, sea level pressure as shown below:

$$p_{sl}(t) = \frac{p(t)}{\left(\frac{p_o}{p_{slo}}\right)} \quad (1)$$

where $p(t)$ represents the uncorrected acoustic pressure measured at altitude, p_o is the static pressure at altitude, and p_{slo} is the standard atmosphere pressure at sea level. Spectra were generated from the corrected composite time history. Time histories are presented in terms of rotor revolution, achieved by normalizing time by the rotor speed. Finally, a sound level metric, SPL_{sl} , was computed by summing the energy in the 1/3-octave bands with center frequencies from 100 Hz to 1000 Hz for each flight condition. This frequency range was considered to encompass the BVI frequencies.

The same procedures for digitizing and averaging were used for the wind tunnel acoustic data reduction for consistency. Since the 80- by 120-Foot Wind Tunnel is near sea level, the correction factor in Eq. (1) is close to unity. The overall sound level metric was also computed for the wind tunnel data.

Nonacoustic Data

Data signals (altimeter, airspeed, outside air temperature, angle of attack, angle of sideslip) from the YO-3A instrumentation boom were digitized at 250 samples/s with no analog filtering over the same time period as the acoustic signals. Mean values were then extracted from the time histories and converted to engineering units using results from an extensive calibration prior to the flight test. The YO-3A rate of descent was determined from the slope of the altimeter signal time history. The helicopter weight at each flight condition was calculated assuming a constant fuel burn rate and the time elapsed from engine start-up to the

midpoint of the data record. Thrust coefficient, tip Mach number, and advance ratio were then computed. The following expressions show the two different methods used for computing tip-path-plane angle in flight:

$$\alpha_{tpp} = \gamma + \theta_f + I_s + a_{1s} \quad (2)$$

$$\alpha_{tpp} = \gamma - \sin^{-1} \left(\frac{0.5 f \mu^2}{C_T \pi R^2} \cos \gamma \right) \quad (3)$$

Equation (2) uses the glide slope angle (γ), the helicopter attitude measured by the gyroscope (θ_f), and the shaft tilt offset angle ($I_s = -5$ deg). The S-76C was not instrumented to measure the longitudinal flapping angle, a_{1s} ; therefore, a_{1s} is not included in the calculations of α_{tpp} . Equation (3), which is based on a simplified force model that excludes non-uniform inflow and pitch and roll moment effects, relies on the equivalent flat plate area ($f = 12.6 \text{ ft}^2$) of the helicopter. In the wind tunnel, the rotor tip-path-plane was taken as perpendicular to the rotor shaft with the first harmonic cyclic flapping set nominally to zero. No corrections for wall effects are applied. Mean tunnel conditions and rotor forces were computed by averaging over the 30 s data acquisition period.

Data Quality

Obtaining acoustic measurements in forward flight while maintaining a tight formation is a difficult procedure. The steadiness and consistency of the measurements depends on pilot skill and the atmospheric conditions. Acoustic measurements in a wind tunnel may be steadier, but are subject to contamination from reflections. The following discussion quantifies some of these sources of unsteadiness and contamination.

Flight Data

The establishment of the flight formation is initiated by the YO-3A pilot. As the lead aircraft, the YO-3A establishes a specified constant forward speed and descent rate. The S-76C pilot visually aligns the tip of the YO-3A tail with a target on the right wing to bring the helicopter into proper angular position. The accuracy of the angular alignment is estimated to be ± 5 deg. While maintaining angular alignment, the S-76C pilot closes in on the YO-3A until the desired separation distance, as measured by the laser rangefinder, is achieved. The accuracy of the rangefinder is approximately ± 2 ft. Once the two aircraft are "on condition," data are recorded for 30 s. The formation passes through the desired altitude approximately midway through the 30 s data record. As much as possible, the S-76C pilot refrains from adjusting controls during data acquisition. For the conditions presented in this paper, the sideslip angle was small (< 3 deg). By studying the recorded separation distances and listening to recorded comments made by both pilots, the steadiest 10 s period is extracted from the 30 s data record and digitized. Each flight condition was acquired at least twice. Flight points that were to be matched with wind tunnel data were acquired three times. This procedure prevented acquiring an extensive matrix of conditions, but did provide a measure of the repeatability of the flight data. For example, Fig. 7 shows repeated flight conditions. Although the magnitudes of some of the peaks in the events vary from Fig. 7(a) to 7(b), the detail of the events repeat with reasonable consistency. A redundant method of computing the tip-path-plane angle was established by using Eqs. (2) and (3). Table 4 shows that the two equations produced values consistent with each other. Tip-path-plane angles shown in all figures were computed using Eq. (3).

The technique for averaging the acoustic time histories discussed earlier can be a source of error. In Ref. 5, this technique worked well in averaging high-speed impulsive noise of a two-bladed rotor which is

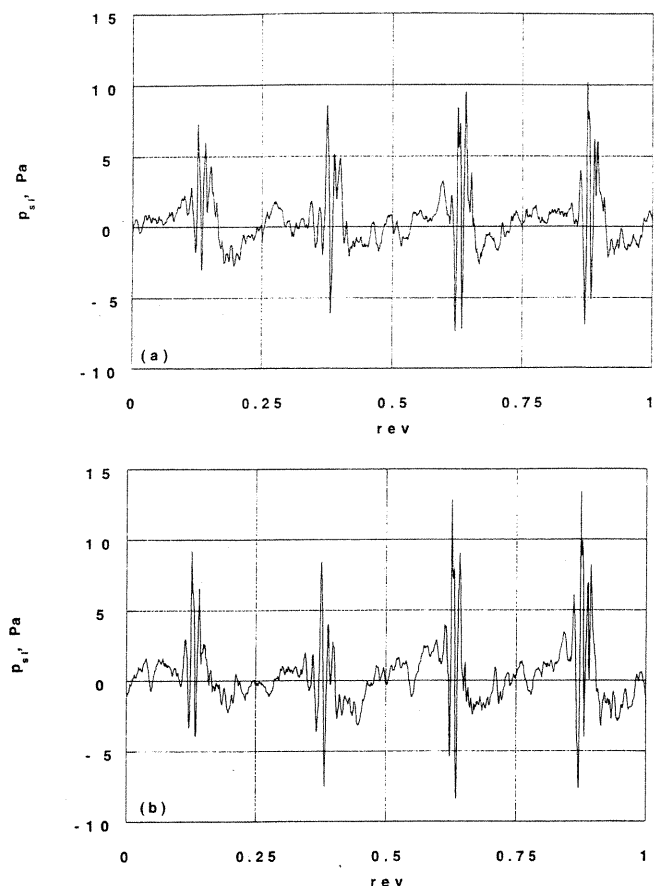


Fig. 7. Repeatability of flight test data (averaged time histories). (a) Flight pt. 304 conditions: $C_T=0.00670$, $M_{tip}=0.615$, $\alpha_{tpp}=6.0$ deg, $\mu=0.167$; (b) Flight pt. 305 conditions: $C_T=0.00667$, $M_{tip}=0.611$, $\alpha_{tpp}=6.4$ deg, $\mu=0.164$.

usually characterized by one large negative pressure peak. BVI noise, however, consists of multiple peaks. The technique works well for waveforms with distinct, repeatable features, but for a four-bladed rotor undergoing weak BVI, selection of an appropriate averaging marker becomes subjective. This difficulty is illustrated in Figs. 8(a) and 8(b) which present an averaged event together with two of the 32 unaveraged events for a weak and strong BVI condition, respectively. The strong BVI condition of Fig. 8(b) is shown for three separate rotor revolutions in Fig. 9. Fig. 8 and 9 give an indication of the variability between the same event from revolution to revolution and also the variability between the four events for different revolutions, respectively.

As discussed earlier, the YO-3A is a relatively quiet aircraft. The background noise of the YO-3A was compared with the measured helicopter noise for the three flight conditions (see Flight points 203, 307, 315 in Table 4) to be compared with wind tunnel data later in this paper. Except for Flight Point 315 at frequencies greater than 1200 Hz, the background noise level was typically 10-20 dB below the S-76C noise level.

Wind Tunnel Data

The test section of the 80- by 120-Foot Wind Tunnel is acoustically treated, with 6-in absorbent lining on the ceiling and floor and 10-in absorbent lining on the walls. The sound absorption coefficient is predicted to be at least 0.9 for frequencies greater than 250 Hz. However, reflection tests revealed the wind tunnel floor caused reflections with magnitudes

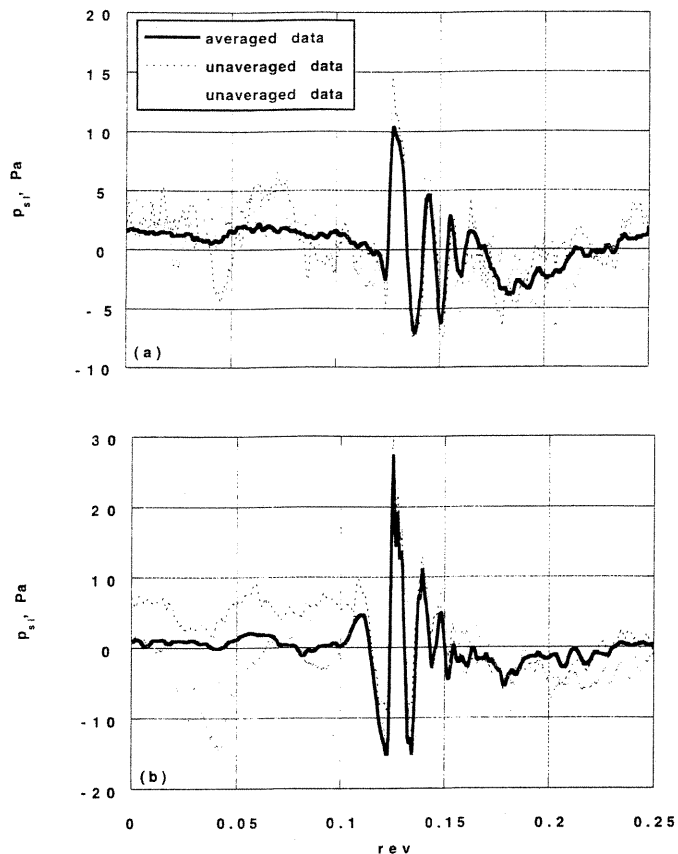


Fig. 8. Averaged and unaveraged flight data for one-quarter of a revolution. (a) Flight pt. 315 conditions: $C_T=0.00600$, $M_{tip}=0.606$, $\mu=0.245$, $\alpha_{tpp}=0.4$ deg; (b) Flight pt. 203 conditions: $C_T=0.00778$, $M_{tip}=0.603$, $\mu=0.164$, $\alpha_{tpp}=5.6$ deg.

about one-half of the single impulsive noise source magnitude. This occasionally caused difficulty in distinguishing between a weak BVI and a reflection. The effect of the wind tunnel floor boundary layer on the acoustic measurements was determined to be unimportant after analyzing data from microphones placed at different heights in the test section.

Averaged and unaveraged wind tunnel data are shown in Fig. 10. Conditions are similar to the flight conditions of Fig. 8. Fig. 10(a) represents a weaker BVI condition than Fig. 10(b). Choosing a repeatable marker for the data of Fig. 10(a) was not possible and so the rotor 1/rev spike was used for averaging. Fig. 11 shows the variability between four BVI events for several revolutions of the data for the strong BVI condition of Fig. 10(b). The measured rotor noise in the wind tunnel was compared with the wind tunnel background noise for the three conditions matching the flight data (see Run 39_24, Run 48_19, and Run 48_18 in Table 4). The background noise includes the RTA and rotating hub (without blades) in addition to the wind tunnel fan drive noise. The background noise was generally 10 dB lower than the rotor noise for frequencies less than 1000 Hz for Run 39_24 and Run 48_19. Run 48_18, the highest advance ratio condition, showed a 10 dB difference only out to approximately 800 Hz.

As discussed earlier, the rotor in the wind tunnel was trimmed by zeroing the 1/rev cyclic flapping angles. In flight, the S-76C pilot trims the rotor propulsive and lift forces while zeroing the helicopter roll and pitching moments. The differences in trim methods may cause slight differences (on the order of 1-2 deg) between the tip-path-plane angle in the wind tunnel and in flight.

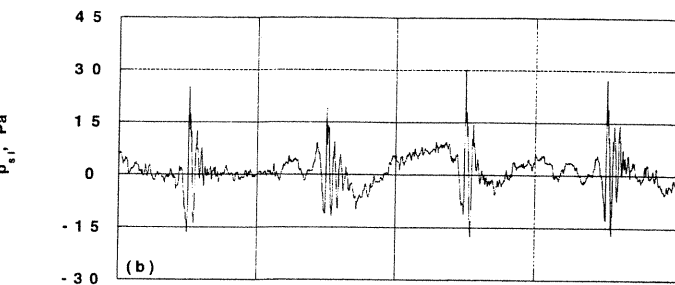
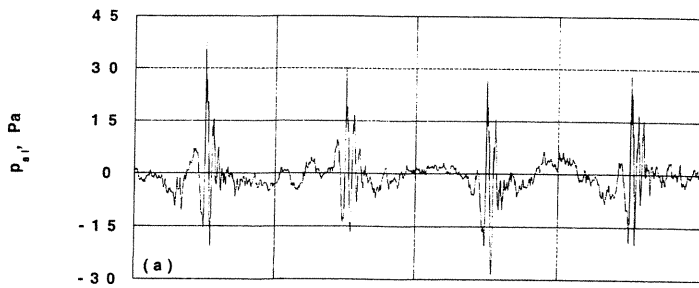


Fig. 9. Variability in unaveraged flight data (full revolution). Flight pt. 203 conditions: $C_T=0.00778$, $M_{tip}=0.603$, $\mu=0.164$, $\alpha_{tip}=5.6$ deg. (a) rev 1 (b) rev 4 (c) rev 20.

Results

Table 4 provides a list of flight conditions including sound levels in SPL_{s1} . Also shown are the wind tunnel conditions which match three of the flight conditions (203, 39_24; 307, 48_19; 315, 48_18). All acoustic flight data presented are from the YO-3A tail microphone. Because of the coarseness of the flight condition matrix, a thorough analysis of parametric effects on BVI noise is not possible. However, some observations are provided on the effects of tip-path-plane angle and advance ratio in the next section, followed by comparisons with wind tunnel data. Although the nondimensional parameters C_T , μ , M_{tip} , and α_{tip} were matched as closely as possible when comparing flight and wind tunnel data, there are other important effects which are difficult if not impossible to measure or control. A primary example is blade tracking. In the wind tunnel, the blades are only tracked for a few specific conditions at one azimuth; therefore, the term "tip-path plane" refers to an idealized plane through the mean path of all four blades. Although the wind tunnel and flight blades are not perfectly tracked for all conditions and azimuths, when analyzing blade-to-blade differences in the data, effects of tracking are assumed small.

Parametric Effects

Fig. 12 shows the effect of increasing tip-path-plane angle while holding the other important nondimensional parameters (C_T , μ , M_{tip}) nearly constant. The effect is similar to that shown for a full-scale and a corre-

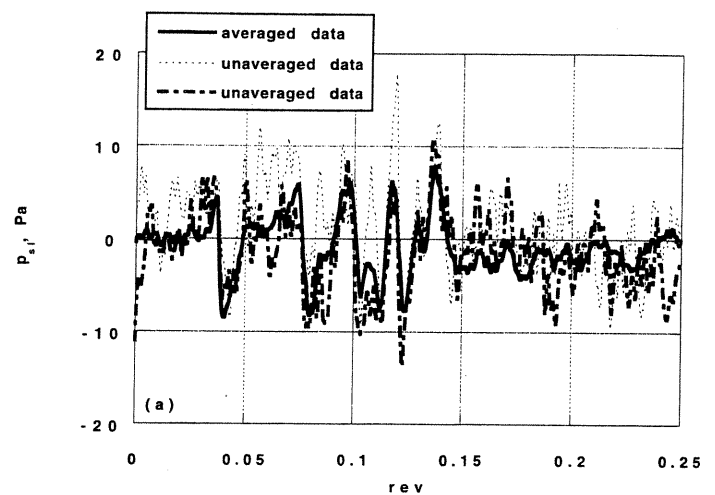
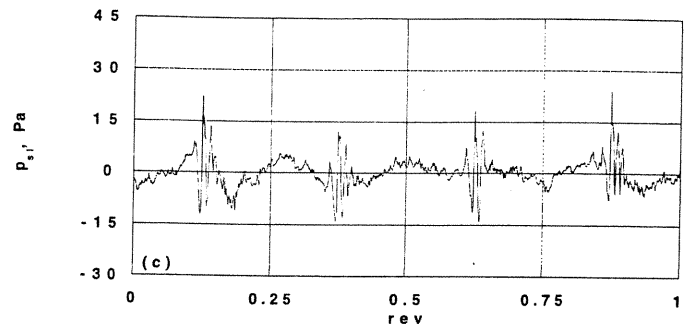


Fig. 10. Averaged and unaveraged data wind tunnel for one-quarter of a revolution. (a) Wind tunnel pt. 48_18 conditions: $C_T=0.00597$, $M_{tip}=0.605$, $\mu=0.251$, $\alpha_{tip}=0.0$ deg; (b) Wind tunnel pt. 39_24 conditions: $C_T=0.00753$, $M_{tip}=0.605$, $\mu=0.173$, $\alpha_{tip}=5.0$ deg.

sponding small-scale two-bladed rotor in Ref. 4. As the tip-path plane is increased, achieved by increasing descent rate, the BVI peaks reach a maximum. Further increases in the tip-path plane angle result in BVI peak reduction.

Fig. 13 shows the effect of increasing μ , achieved by increasing forward speed and descent rate simultaneously in order to maintain a nearly constant α_{tip} . Fig. 13(a) reveals some secondary BVI not evident in Fig. 13(b). A possible explanation is that the rotor wake geometry is not as stable at the lower advance ratio compared to the higher advance ratio case, causing more inconsistent BVI. The blade-to-blade differences in Fig. 13(a) are much more noticeable than in Fig. 13(b). Also, the magnitude of the BVI is increased by 2.3 SPL_{s1} at the higher advance ratio (compare flight points 308 and 315 in Table 4).

Comparisons with Wind Tunnel Data

Following the practice of previous studies, the flight and wind tunnel data are compared in the time domain. Three matching conditions are presented in Figs. 14, 15, and 16 corresponding to low, moderate, and high advance ratio cases, respectively.

Figures 14(a) and 14(b) compare averaged waveforms for a low speed, strong BVI case for one revolution and one-quarter revolution, respec-

Table 4. Flight and wind tunnel test conditions.

Test point	V _D (ft/min)	M _{tip}	V _{true} (kts)	μ	C _T	P _o /P _{slo}	α _{tip} ² (deg)	α _{tip} ³ (deg)	SPL _{st}
Flight									
203 ^a	748	0.603	65.8	0.164	0.00778	0.7857	6.3	5.6	106.2
208	585	0.614	100	0.244	0.00675	0.8512	0.5	1.2	109.6
209	870	0.607	100	0.246	0.00682	0.8557	1.8	2.8	105.4
304	843	0.615	68.4	0.167	0.00670	0.8199	5.6	6.0	101.2
305	863	0.611	66.8	0.164	0.00667	0.8293	5.7	6.4	102.7
306	272	0.605	80.0	0.196	0.00608	0.9244	-0.3	0.4	99.9
307 ^b	306	0.606	82.7	0.203	0.00605	0.9227	0.1	0.5	100.3
308	250	0.606	76.9	0.189	0.00600	0.9272	0.2	0.4	101.4
309	438	0.608	82.5	0.202	0.00601	0.9152	0.8	1.4	103.1
312	868	0.604	78.4	0.193	0.00608	0.9050	4.3	4.8	101.2
315 ^c	490	0.606	100	0.245	0.00600	0.9017	-0.4	0.4	103.7
Wind tunnel									
39_24 ^a	741	0.605	69.0	0.173	0.00753	1.0045	5.0 ¹		105.0
48_17	473	0.604	100	0.251	0.00598	1.0041	0.0 ¹		104.9
48_18 ^c	475	0.605	100	0.251	0.00597	1.0041	0.0 ¹		104.9
48_19 ^b	245	0.605	79.9	0.200	0.00599	1.0041	0.0 ¹		102.6

¹ shaft angle
² from Eq. (2)
³ from Eq. (3)

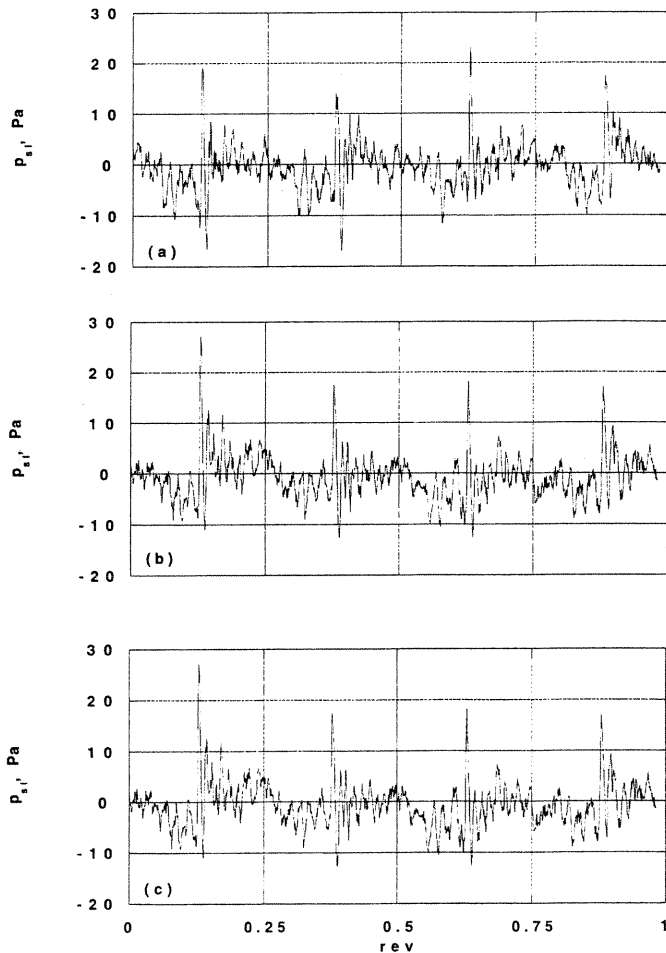


Fig. 11. Variability in unaveraged data wind tunnel data (full revolution). Wind tunnel pt. 39_24 conditions: C_T=0.00753, M_{tip}=0.605, μ=0.173, α_{tip}=5.0 deg. (a) rev 1 (b) rev 15 (c) rev 30.

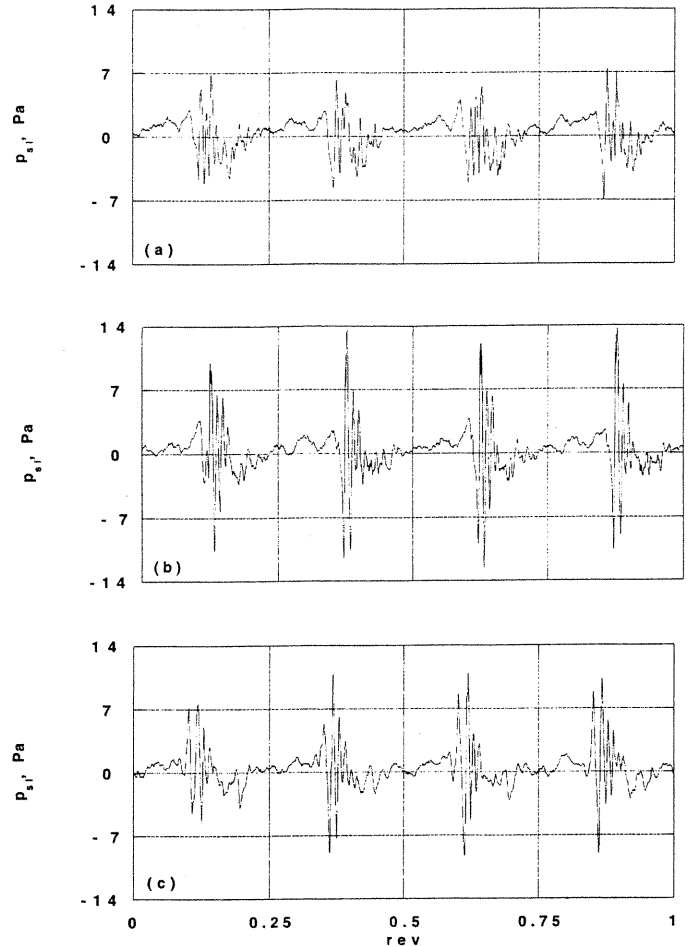


Fig. 12. Effect of α_{tip} on BVI flight data (averaged time histories). (a) Flight pt. 306 conditions: C_T=0.00608, M_{tip}=0.605, μ=0.196, α_{tip}=0.4 deg. (b) Flight pt. 309 conditions: C_T=0.00601, M_{tip}=0.608, μ=0.202, α_{tip}=1.4 deg. (c) Flight pt. 312 conditions: C_T=0.00608, M_{tip}=0.604, μ=0.193, α_{tip}=4.8 deg.

tively. Because of the slight differences in rotor rpm during the flight and wind tunnel tests, the two waveforms have been aligned a quarter revolution at a time. The similarity in the peak widths is quite good, although the peaks in the flight data appear greater in magnitude generally. The noise level measured in flight is slightly (1.2 SPL_s) higher than the level measured in the wind tunnel (compare flight point 203 and wind tunnel point 39_24 in Table 4). The flight data show three to four vortex interactions per blade. The wind tunnel data also show this; however, multiple lower level pulses are also clearly evident. There are several negative peaks prior to the major BVI and several positive peaks following the major BVI. This pattern is repeated for all four blades in the wind tunnel. Analysis of the reflection test data indicate that some of the low level pulses following the major BVI may be due to floor reflections, while the smaller pulses preceding the major BVI may be caused by ceiling reflections and/or weak primary vortex interactions.

The pulse width, together with the blade-vortex miss distance, is an indication of the core size of the vortex filament interacting with the blade. Figure 14(b) reveals that the pulse widths of the flight and wind tunnel data are very similar. This is not surprising since two similar full-scale rotors are being compared and the viscous effects should be directly comparable. Reproducing full-scale viscous effects using small-scale models is always a concern because of Reynolds number effects.

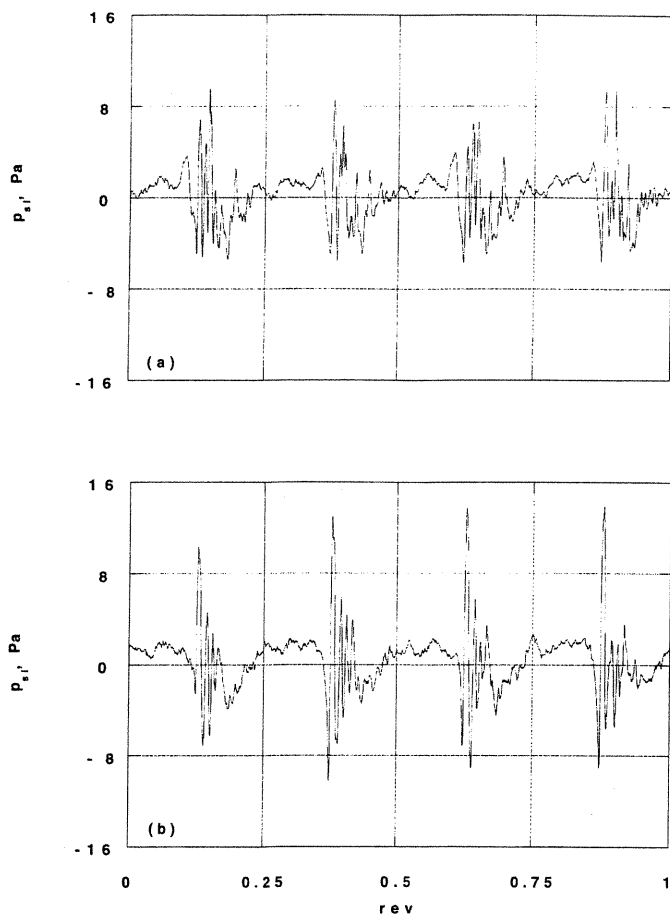


Fig. 13. Effect of advanced ratio on BVI flight data (averaged time histories). (a) Flight pt. 308 conditions: $C_T=0.00600$, $M_{tip}=0.606$, $\alpha_{tip}=0.4$ deg, $\mu=0.189$; (b) Flight pt. 315 conditions: $C_T=0.00600$, $M_{tip}=0.606$, $\alpha_{tip}=0.4$ deg, $\mu=0.245$.

The similarity in pulse widths also indicates that the tip-path-plane angle in the wind tunnel and in flight were similar despite the difference in trim methods.

A frequency spectrum of the flight data showed the characteristic BVI feature (energy spikes at blade passage harmonics inside a scalloped envelope) out to 2000 Hz. The wind tunnel spectrum envelope was not as clean, possibly due to reflections. The flight noise levels were generally higher for frequencies greater than 600 Hz compared with the wind tunnel noise levels.

A moderate advance ratio condition is shown in Fig. 15. Compared to Fig. 14, this condition is for a much lower thrust coefficient. Major peak widths match well, although magnitudes differ by as much as 5 Pa or more. Table 4 shows that the flight noise level is 2.3 SPL_{sl} lower than the wind tunnel level (compare flight point 307 and wind tunnel point 48_19). The wind tunnel data again display the lower level impulses adjacent to the major BVI, although the impulses are not as prominent compared to Fig. 14.

Fig. 16 represents the highest advance ratio condition of the three matched cases. Conditions are similar to Fig. 15 except for advance ratio. The noise level in flight is 1.2 SPL_{sl} lower than the wind tunnel level (compare flight point 315 and wind tunnel point 48_18 in Table 4). Although the two waveforms are presented overlaid, no attempt was

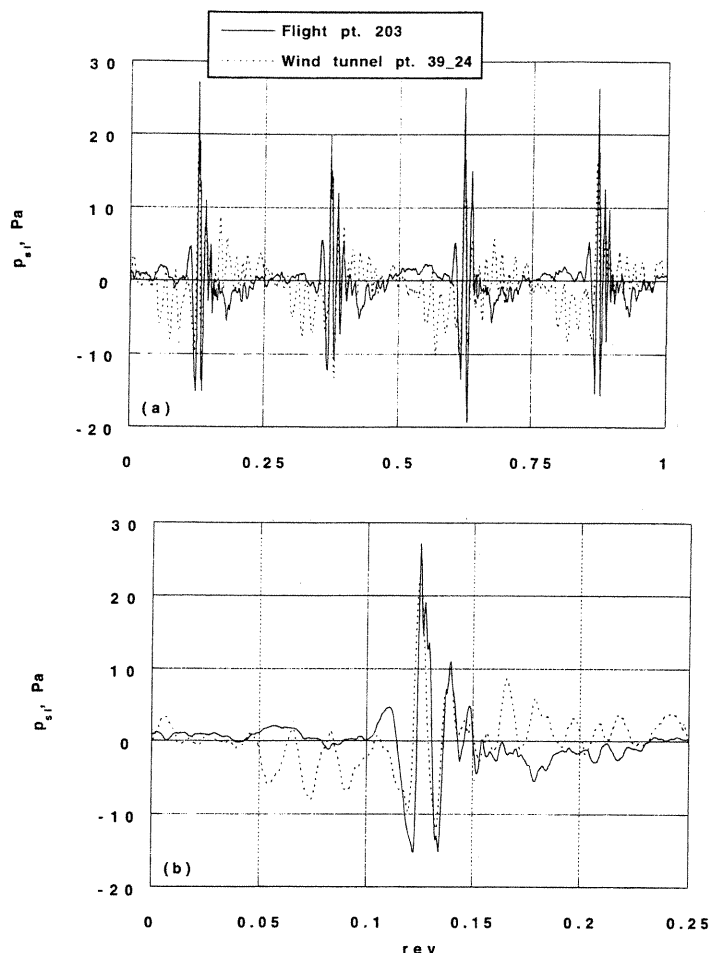


Fig. 14. Flight and wind tunnel data (averaged time histories) comparison. Flight pt. 203 conditions: $C_T=0.00778$, $M_{tip}=0.603$, $\mu=0.164$, $\alpha_{tip}=5.6$ deg. Run 39_24 conditions: $C_T=0.00753$, $M_{tip}=0.605$, $\mu=0.173$, $\alpha_{tip}=5.0$ deg. (a) one revolution (b) 1/4 revolution.

to align the two waveforms in time since the shapes are so different. Also, averaging the wind tunnel data using the technique described earlier was impossible due to blade-to-blade and revolution-to-revolution differences in the data. Instead, the wind tunnel data were averaged using the rotor 1/ rev signal. Differences in averaging methods are possibly contributing to the poor comparison shown in Fig. 16. In addition, the signal-to-noise ratio in flight and in the wind tunnel was worse compared to the lower speed cases, further adding to the poor comparison shown in Fig. 16.

Waveforms were analyzed in detail for each one-quarter revolution of the wind tunnel and flight test data, respectively, shown in Fig. 16. Similar features existed in each quarter of a revolution of the wind tunnel data, but appeared highly distorted from one blade to another. The blades in flight, however, experienced similar interactions with the rotor wake. For this condition, the 80- by 120-Foot Wind Tunnel environment was not an adequate substitute for the free-air environment. Interestingly, Ref. 6 observed a deterioration in the scalability of BVI noise at high advance ratios ($\mu > 0.22$). The possibility of the data from 48_18 simply being invalid (instrumentation problems or data acquisition and reduction errors) is very small, considering that data from 48_19 was acquired immediately after 48_18 and shows blade-to-blade similarities and reasonable agreement with the flight data (Fig. 15). In addition, Table 4 shows that the wind tunnel conditions for 48_18 were repeated,

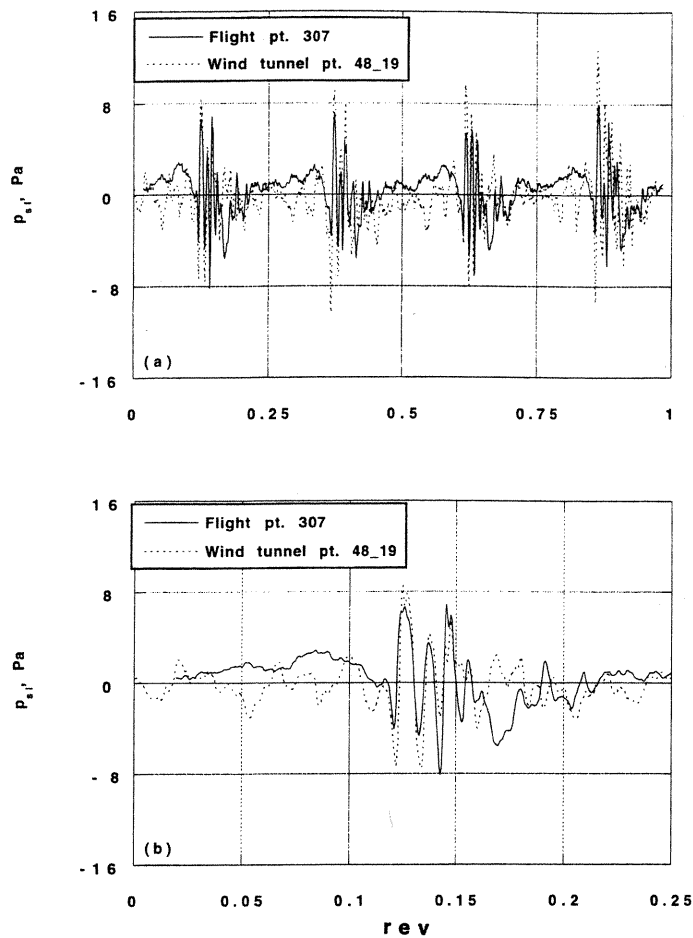


Fig. 15. Flight and wind tunnel data (averaged time histories) comparison. Flight pt. 307 conditions: $C_T=0.00605$, $M_{tip}=0.606$, $\mu=0.203$, $\alpha_{tip}=0.5$ deg. Run 48_19 conditions: $C_T=0.00599$, $M_{tip}=0.605$, $\mu=0.200$, $\alpha_{tip}=0.0$ deg. (a) one revolution (b) 1/4 revolution.

with consistent results, in 48_17.

Conclusions

In-flight acoustic measurements of an S-76C helicopter were acquired using the NASA Ames YO-3A research aircraft. Within the context of the limited flight test matrix, parametric effects on BVI noise are discussed. Comparisons with full-scale wind tunnel data are also shown. Specific findings include:

1. For the low and moderate advance ratio conditions presented, the BVI pulse widths of the flight and wind tunnel data were very similar, indicating the conditions were well-matched.
2. The small impulses immediately preceding and following major BVI in the wind tunnel data did not appear in the flight data and were likely caused by reflections and/or weak primary vortex interactions.
3. Comparisons between the flight and wind tunnel data waveforms for the high advance ratio case ($\mu \approx 0.25$) were poor. For this condition, the wind tunnel data showed greater blade-to-blade and revolution-to-revolution variability than the flight data. The lack of agreement at this advance ratio was also observed in previous comparisons of small-scale wind tunnel data with flight data.
4. Noise levels measured in the wind tunnel are within 2.5 SPL_{sl} of the

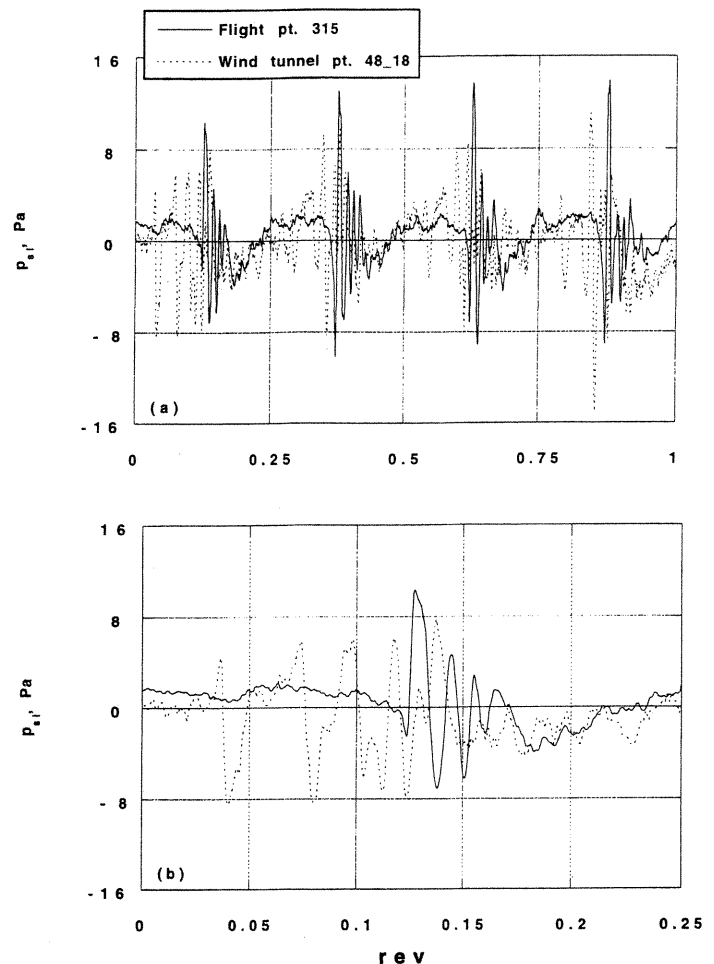


Fig. 16. Flight and wind tunnel data (averaged time histories) comparison. Flight pt. 315 conditions: $C_T=0.00600$, $M_{tip}=0.606$, $\mu=0.245$, $\alpha_{tip}=0.4$ deg. Run 48_18 conditions: $C_T=0.00597$, $M_{tip}=0.605$, $\mu=0.251$, $\alpha_{tip}=0.0$ deg. (a) one revolution (b) 1/4 revolution.

levels measured in flight.

5. For the flight conditions presented, the BVI peaks increased with increasing tip-path-plane angle until reaching a maximum. Further increases in the tip-path plane angle resulted in BVI peak reduction. These observations were also observed in two-bladed rotor flight test data and small-scale data.
6. Increasing advance ratio increases the magnitude of the BVI noise for the flight conditions presented.

Acknowledgements

The authors thank Dr. Marianne Mosher and Dr. Fred Schmitz of NASA Ames Research Center for their valuable advice regarding the analysis of the data. The contributions of Mr. Martin Hagen and Mr. Cahit Kitaplioglu of NASA Ames Research Center are acknowledged for their work in the acquisition of S-76 rotor acoustic data in the 80- by 120-Foot Wind Tunnel. The efforts of many people from NASA Ames and Sikorsky Aircraft contributed to this successful flight test program. In particular, the efforts of the following people are greatly appreciated: Dan Hoang, NASA Ames, YO-3A Instrumentation Engineer; Munro Dearing, NASA Ames, YO-3A Pilot; George Tucker, NASA Ames, S-76C Co-Pilot; Tom Davis, Sikorsky Aircraft, S-76C Pilot.

References

¹Schmitz, F. H. and Boxwell, D. A., "In-Flight Far-Field Measurement of Helicopter Impulsive Noise," American Helicopter Society 32nd Annual Forum, Washington, D. C., May 1976.

²Vause, C. R., Schmitz, F. H., and Boxwell, D. A., "High-Speed Helicopter Impulsive Noise," American Helicopter Society 32nd Annual Forum, Washington, D. C., May 1976.

³Boxwell, D. A. and Schmitz, F. H., "Full-Scale Measurements of Blade-Vortex Interaction Noise," American Helicopter Society 36th Annual Forum, Washington, D. C., May 1980.

⁴Schmitz, F. H., Boxwell, D. A., Lewy, S., and Dahan, C., "Model-to Full-Scale Comparisons of Helicopter Blade-Vortex Interaction Noise," *Journal of the American Helicopter Society*, Vol. 29, (2), Apr 1984.

⁵Splettstoesser, W. R., Schultz, K. J., Schmitz, F. H., and Boxwell, D. A., "Model Rotor High-Speed Impulsive Noise-Parametric Variations and Full-Scale Comparisons," American Helicopter Society 39th Annual Forum, St. Louis, Missouri, May 1983.

⁶Splettstoesser, W. R., Schultz, K. J., Boxwell, D. A., and Schmitz, F. H., "Helicopter Model Rotor-Blade Vortex Interaction Impulsive Noise: Scalability and Parametric Variations," Tenth European Rotorcraft Forum, The Hague, The Netherlands, Aug 1984.

⁷Splettstoesser, W. R., Schultz, K. J., and Martin, R. M., "Rotor Blade-Vortex Interaction Impulsive Noise Source Identification and Correla-

tion with Rotor Wake Predictions," AIAA-87-2744, AIAA 11th Aeroacoustics Conference, Palo Alto, California, Oct 1987.

⁸Martin, R. M., Splettstoesser, W. R., Elliot, J. W., and Schultz, K. J., "Advancing-Side Directivity and Retreating-Side Interactions of Model Rotor Blade-Vortex Interaction Noise," NASA TP 2784, AVSCOM TR 87-B-3, May 1988.

⁹Burley, C. L. and Martin, R. M., "Tip-Path-Plane Angle Effects on Rotor Blade-Vortex Interaction Noise Levels and Directivity," American Helicopter Society 44th Annual Forum, Washington, D. C., Jun 1988.

¹⁰Martin, R. M., Marcolini, M. A., Splettstoesser, W. R., and Schultz, K. J., "Wake Geometry Effects on Rotor Blade-Vortex Interaction Noise Directivity," NASA TP 3015, Aug 1990.

¹¹Marcolini, M. A., Martin, R. M., Lorber, P. F., and Egolf, T. A., "Prediction of BVI Noise Patterns and Correlation with Wake Interaction Locations," American Helicopter Society 48th Annual Forum, Washington, D. C., Jun 1992.

¹²Cross, J. L. and Watts, M. E., "Tip Aerodynamics and Acoustics Test," NASA RP 1179, Dec 1988.

¹³Cross, J. L., "YO-3A Acoustics Research Aircraft Systems Manual," NASA TM 85968, Jul 1984.

¹⁴Cross, J. L. and Watts, M. E., "In-Flight Acoustic Testing Techniques Using the YO-3A Acoustic Research Aircraft," NASA TM 85895, Feb 1984.

¹⁵Watts, M. E., "ALDAS User's Manual," NASA TM 102381, Apr 1991.